Natural Resources Canada | Ressources naturelles Canada

GEOLOGICAL SURVEY OF CANADA
OPEN FILE 8124

Icings in the Lac la Martre area (1984–2015), Northwest Territories, mapped from Landsat imagery

C.S. Fish, P.D. Morse, and S.A. Wolfe

2017

GEOLOGICAL SURVEY OF CANADA
OPEN FILE 8124

Icings in the Lac la Martre area (1984–2015), Northwest Territories, mapped from Landsat imagery

C.S. Fish, P.D. Morse, and S.A. Wolfe

Geological Survey of Canada, 601 Booth St., Ottawa, Ontario

2017

doi:10.4095/299737

This publication is available for free download through GEOSCAN (http://geoscan.nrcan.gc.ca/).

Recommended citation
Fish, C.S., Morse, P.D., and Wolfe, S.A., 2017. Icings in the Lac la Martre area (1984–2015), Northwest Territories, mapped from Landsat imagery; Geological Survey of Canada, Open File 8124, 1 .zip file. doi:10.4095/299737

Publications in this series have not been edited; they are released as submitted by the author.

ABSTRACT

Icings are sheet-like masses of layered ice that form over the winter by freezing of successive flows of water on the ground surface or on top of river or lake ice. Icings can negatively impact the performance of seasonal and all-season roads and are a transportation risk in Arctic regions. Therefore, maps of their occurrence and reoccurrence provide important geoscience information required for development and transportation infrastructure planning. In this study, a set of icing maps was derived using threshold values of band ratios from a time series of Landsat images (1984 – 2015), located within the Bear and Interior Platform Geological Provinces in the Lac la Martre area, NWT (WRS-2 Path 49/Row 16). The icings maps were generated using images acquired in late spring when the region is largely snow-free, but ice bodies remain. A water mask created from summer images was used to differentiate between different types of frozen water bodies (rivers, lakes, icings), so any remaining ice was considered to be icings. Icing reoccurrence maps were generated by overlaying successive icing distribution maps in a Geographic Information System. This Open File contains the digital, georeferenced icing data.

DISCLAIMER

Her Majesty the Queen in right of Canada, as represented by the Minister of Natural Resources ("Canada"), does not warrant or guarantee the accuracy or completeness of the information ("Data") and does not assume any responsibility or liability with respect to any damage or loss arising from the use or interpretation of the Data.

The Data are intended to convey regional trends and should be used as a guide only. The Data should not be used for design or construction at any specific location, nor are the Data to be used as a replacement for site-specific geotechnical investigations.

TABLE OF CONTENTS

LIST OF FIGURES

LIST OF TABLES

1 INTRODUCTION

The remote community of Whati, Northwest Territories, is one of many northern communities that rely on seasonal roads or ice roads for accessibility. Currently, an all-season road is planned to connect Whati to other communities. Developing infrastructure corridors in the North lends itself to many challenges and considerations, one of which is the development of icings. Icings (a.k.a. aufeis, naled, flood ice, flood-plain icing, overflow ice, "glaciations" in the colloquial, and "kw'ôö" in the local Tåîchô dialect) are layered masses of ice, which form due to successional freezing of groundwater flow on the surface (Morse *et. al*., 2015). These icings pose a risk to infrastructure and transportation as they can negatively impact bridges and culverts and decrease road safety (Carey, 1973). Additionally, icing development affects northern affairs such as water resource management (Kane and Slaughter, 1973; Reedyk *et al*., 1995; Li *et al*., 1997), and flooding hazards (Prowse, 1995).

In 2014 (Morse *et al*., 2014), the Geological Survey of Canada (GSC), Natural Resources Canada, used remotely sensed data from the Landsat series of satellites to produce a map of regional icing distribution and dynamics for the Great Slave region. Here, we apply that methodology to map icings in an adjacent Landsat image, covering the Lac la Martre area, Northwest Territories (Figure 1). The remotely sensed images, available from 1984 to the present, were collected from ideally cloud-free, late spring days when snow has melted and icings remained. At such a time, icings are visually distinct (*c.f.* Yoshikawa *et al*., 2007). The imagery was manipulated using band ratios and threshold values in order to isolate and map icings on land. A final map was generated using a Geographic Information System (GIS) in which the land-fast icing data is combined and mapped over a number of years. With this methodology, the distribution and frequency of icing development can be identified, interpreted, and compared to local climatic and hydrologic data. This work is part of research conducted at the GSC through the PHASAR (Permafrost and Hydrology in Arctic and Sub Arctic Regions) activity. This Open File contains the GIS-ready georeferenced digital icing data.

1.1 Icings

Icings are a winter hydrological phenomenon typical of northern streams and rivers (Figure 2). Icing occurrence and process dynamics are influenced by climate, hydrology, geology, permafrost, and topography (Carey, 1973; Kane, 1981). Consequently, conditions most favourable for icing formation are severe continental climate, cold winters with low snow cover, the presence of groundwater springs or unfrozen, water bearing layers (taliks), and highly permeable materials such as deposits of sand or gravel, organic matter, or karst terrain (Romanovskii *et al*., 1996). Icings form when water in a stream channel becomes pressurized and flows onto existing ice cover or the ground (Kane, 1981). Overflow occurs when hydrostatic head rises, in either subpermafrost groundwater or water from near-surface taliks, in association with or following periods of increased (though still subfreezing) air temperature. In general, the icing thickness/volume is in direct relation to the water source volume (Veillette and Thomas, 1979; Kane, 1981; Yoshikawa *et al*., 2007). Repeated flow events throughout the winter increase the ice thickness, such that by the end of the cold season the channel and adjacent floodplain may fill completely with ice. Icings may be classified by differing water sources, and may be detected and delineated using various spectral signatures (Morse *et al.*, 2014). As the extent of an icing may be different or non-existent in successive years, a single-year map of icing distribution does not capture the icing dynamics. An alternative approach is to map icings over a number of years to capture the overall distribution (Dean, 1984). These data can then be analyzed in a GIS to determine the icing return frequencies.

Figure 1. Location of the study area (Landsat WRS-2 Path 49/Row 16) is indicated by the black square over the Lac la Martre region, Northwest Territories.

Figure 2. Icing example from the Great Slave Upland High Boreal Ecoregion

1.2 Satellite Mapping of Icing Distribution

Satellite mapping of icings has been undertaken in Canada in the Yellowknife region, NWT, (Morse *et al.*, 2014) but the focus of mapping efforts in North America has been almost entirely on the North Slope of Alaska (Harden *et al*., 1977; Hall and Roswell, 1981; Dean, 1984; Li *et al*., 1997; Yoshikawa *et al*., 2007). Icing location, shape, and area are easily interpreted from satellite images taken in late spring following snowmelt because it is possible to distinguish between water and ice due to variations in reflectance and emittance of electromagnetic (EM) radiation between liquid and solid water [*e.g*., Landsat (Harden *et al*., 1977; Hall and Roswell, 1981; Dean, 1984; Yoshikawa *et al*., 2007); synthetic aperture radar (SAR) (Li *et al*., 1997; Yoshikawa *et al*., 2007)]. Some of the benefits of Landsat data over SAR data are the length of continuous record (1984 to present), relatively high spatial resolution (30 m), large scene-area (~ 170 km × 185 km), and free availability (http://glovis.usgs.gov/). Here, we apply a semi-automated mapping approach developed by Morse *et al*. (2014) to map icings in the Lac la Martre area.

1.3 Regional Setting

Meteorological data for the region are sparse. The longest continuous record comes from Yellowknife, NWT (Environment Canada, 2016), about 150 km away. The regional climate is strongly continental (Figure 3), with cold winters (-25.6°C January mean temperature) and relatively warm summers (17.0 July mean temperature). Nearly 76% of the annual precipitation (289 mm) falls as rain from May to November, with scant snowfall over the winter months. Beginning in September, snow accumulates steadily throughout the winter until March when the month-end snow depth is 37 cm. Snowmelt is largely complete by the end of April, with total ablation by the end of May. The study area, located in the extensive discontinuous permafrost zone (Heginbottom *et al*., 1995), is divided into ten ecoregions of the Taiga Plains and Taiga Shield (Figure 4) (Ecosystem Classification Group, 2007; 2008). From northwest to southeast they are: (i) the Lac Grandin Upland Low Subarctic (LGULS); (ii) the Lac Grandin Plain Low Subarctic (LGPLS); (iii) the Bulmer Plain Low Subarctic (BPLS); (iv) The Great Slave Lowland High Boreal (GSLHB); (v) the Great Slave Upland High Boreal (GSUHB): (vi) the Great Slave Plain High Boreal (GSPHB); (vii) the Horn Slopes Low Subarctic (HSLS); (viii) the Horn Plateau Low Subarctic (HPLS); (ix) the Horn Slopes Mid Boreal (HSMB); and (x) the Great Slave Lowland Mid Boreal (GSLMB). Ecoregion characterization and description from Ecological Regions of the Northwest Territories—Taiga Plains and Ecological Regions of the Northwest Territories—Taiga Shield (2007, 2008) are summarized as follows:

Lac Grandin Upland Low Subarctic

The LGULS ecoregion is comprised of two isolated hills over 500 mASL with only the southern upland included in the study area. Characterized by hummocky and rolling medium- to fine-textured till terrain underlain by cretaceous marine shales, this ecoregion has limited permafrost occurrence. The forest is a patchwork of trembling aspen stands, mixed stands of aspen, white spruce, and early successional dwarf birch and willow shrublands where there have been recent burns. Small circular pothole lakes are numerous and peat plateaus, slope fens, northern ribbed fens and spring fens occur in depressions and along lower slopes.

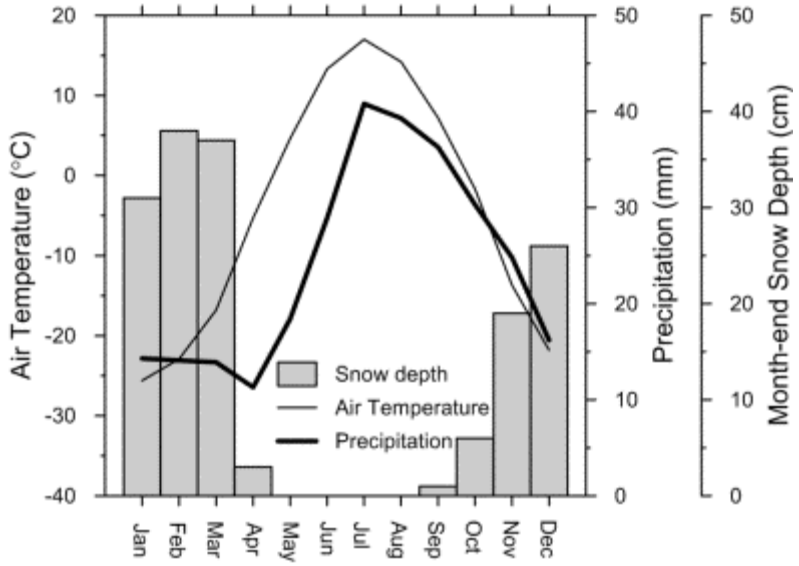

Figure 3. Climate normals (1981-2010) at Yellowknife Airport, Northwest Territories.

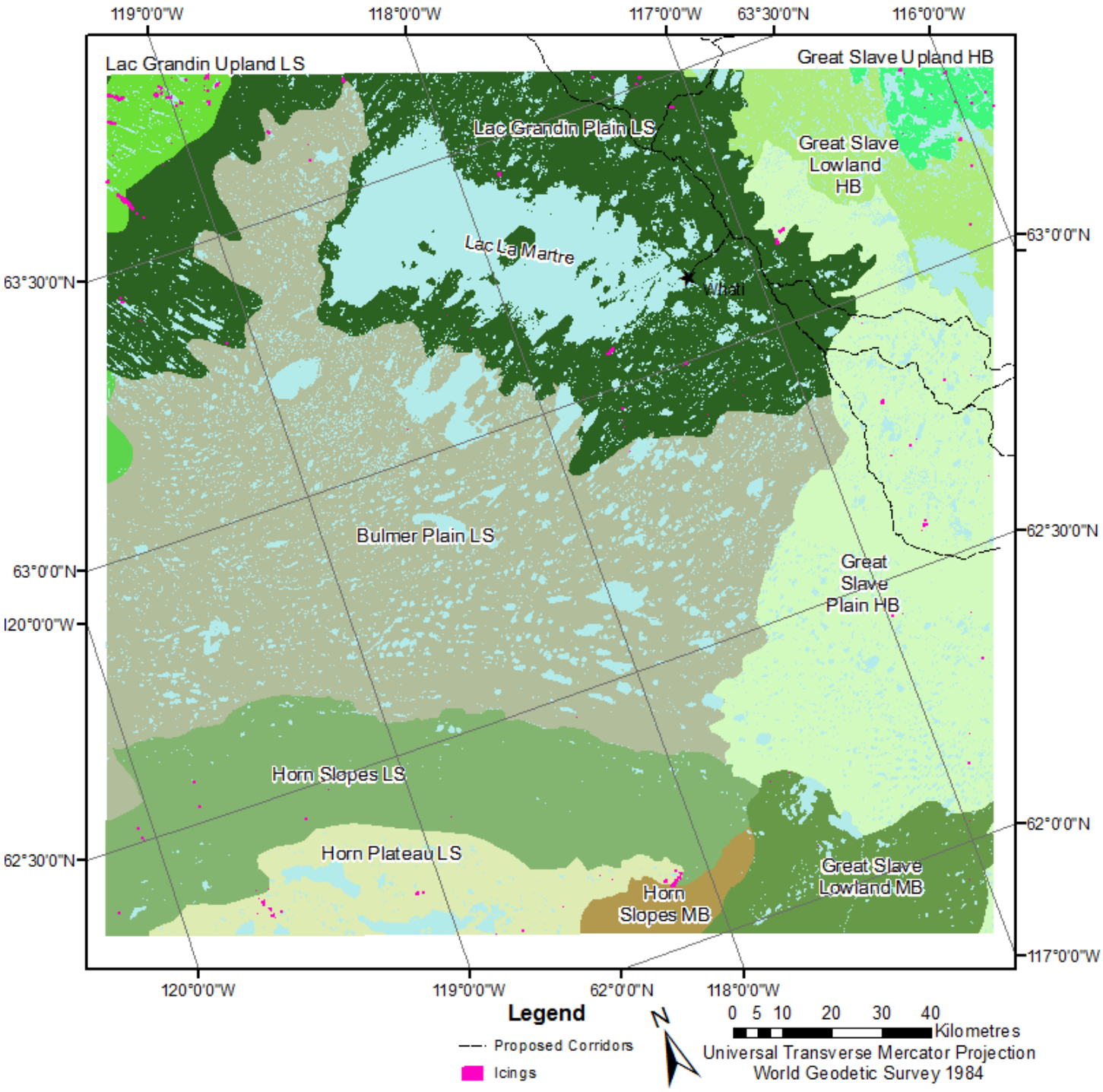

Figure 4. Ecoregions in the Yellowknife area overlain by a composite distribution of icings (1984 to 2014) digitally mapped from Landsat 5,7,8 (E)TM(+)/OLI sensors (WRS-2 Path 49/Row 16).

Lac Grandin Plain Low Subarctic

The LGPLS is a complex glacial landscape of fluted and hummocky terrain generally sloping towards the northeast, but with local topographic variations of up to 200m. Elevations range from 175 to 600 mASL. Cambrian-Devonian limestones and dolomites underlie much of the ecoregion and are exposed as karst topography (sinkhole lakes) and horizontally-bedded strata. This limestone influences the local vegetation and provides the parent material for much of the local hummocky, calcareous, and bouldery till. Frequently burned, this ecoregion is host to a complex mix of regenerating shrubs, young jack pines, and deciduous stands of white birch and trembling aspen. The heavily fluted south west corner of the ecoregion has some of the tallest and most diverse forest in the area.

Bulmer Plain Low Subarctic

The BPLS is dominated by flat, recently burned, peat plateaus and a dense network of shallow calcareous lakes. About 65% of this area is covered by peat plateaus, with boulder glacial till overlying bedrock. This terrain has produced simple, characteristic sequences of regenerating spruce bog with slow growing black spruce seedlings, northern and common Labrador tea, cloud berry, and sparse lichen. Underlying this ecoregion is horizontally bedded dolomite, limestone, and sandstone of Cambrian-Devonian age which provides the parent material in solution for calcium carbonate deposits on the bottom and along shorelines of shallow ponds.

Great Slave Lowland High Boreal

The GSLHB is a nearly-level Precambrian granitoid bedrock plain with extensive, discontinuous wave-washed tills, lacustrine deposits, and glaciofluvial materials occurring between outcrops and in bedrock fractures where wetlands are common (Kerr and Wilson, 2000). The northern boundary of GSKHB roughly coincides with the limit of extensive sediment infilling. Elevations within GSKHB range from about 160 to 200 mASL, with A wide array of forest types occur, ranging from mixed conifer, to conifer-deciduous, to pure white birch stands. Jack pine and aspen forests are widespread on well drained areas. Shore and floating fens are vegetated with shrubs and sedge, and peat plateaus that occur in wet depressions commonly have collapse scars.

Great Slave Upland High Boreal

The GSUHB ecoregion is a nearly-level Precambrian sedimentary bedrock plain with few hill systems, with elevations that range from about 200 to 300 mASL, and a few local promontories. The gentle southwest-slope has thin discontinuous till veneers and scattered outwash deposits. Thin, discontinuous deposits of wave-washed tills, glaciolacustrine sediments, and glaciofluvial materials occur in rock fractures and between outcrops as a consequence of Glacial Lake McConnell which reached a maximum elevation of about 290 mASL, covering most of the ecoregion (Kerr and Wilson, 2000). These deposits are a sufficiently thick substrate for discontinuous black spruce and jack pine forests to occur.

Great Slave Plain High Boreal

The GSPHB is characterized by a gentle, dome-shaped topography, underlain by horizontally bedded dolomite, limestone and sandstone of Cambrian to Devonian age. Frequently burned, this dry, well-drained plain, capped by washed till through the centre of the region, is forested by extensive young jack pine stands and white spruce that grow adjacent to small streams and wetlands. Concentric, coarse-textured beach ridges formed post-glacially with as a result of a receding shoreline due to isostatic uplift. The limestone exposures, karst topography, shallow marl ponds, and numerous beach ridges are rarely seen elsewhere in the Northwest Territories and make this a distinctive ecoregion.

Horn Slopes Low Subarctic

The HSLS is a gently sloped, north facing ecoregion characterized by undulating to hummocky medium- to fine-textured boulder till with organic veneers and blankets covering between 30 and 50 percent of the landscape. Regenerating dwarf birch is widespread due to a recent forest fire, with white and black spruce stands along stream channels. Numerous episodic streams drain downslope from the Horn Plateau LS, which may be fed by seepage from the upper Cretaceous marine shales and conglomerates that underlie the region. Because of the low sun angles associated with a northern aspect at this latitude, this ecoregion displays patterns of vegetation, soil and permafrost typical of a colder climate.

Horn Plateau Low Subarctic

The HPLS ecoregion is a nearly level undulating to hummocky till plateau that rises more than 400m above the surrounding plains, with boundaries defined by slope breaks. Organic material blankets the gently undulating or level till and covers between 30 and 50 percent of the ecoregion. Most of the Horn Plateau has burned within the last 25 years, resulting in vegetation consisting of regenerating shrublands, dwarf birch, and fire-successional jack pine. Locally common on the level areas and eastern half of the ecoregion are nearly treeless polygonal peat plateaus; they are the dominant wetland type due to colder local climate at higher elevations.

Horn Slopes Mid Boreal

The HSMB ecoregion encompasses the gently to steeply inclined south-facing slopes of the Horn Plateau and experiences relatively warm temperatures due to the slopes' sun exposure. Slope failure and therefore mass movements of soil are frequent due to steep slopes and groundwater seepage from underlying Upper Cretaceous marine shales and conglomerates. This seepage, along with dozens of small streams, feeds a belt of fens along the slope base. Colluvium deposits are found on or below the slumped areas and make up 30 to 40 percent of the ecoregion. As with many of the surrounding ecoregions, the landscape shows evidence of being recently burned, with young deciduous forests, shrub lands, and scattered stands of mature white spruce.

Great Slave Lowland Mid Boreal

The GSLMB ecoregion is an expanse of nearly flat wetlands, with only the northernmost part of the large ecoregion extending into the study area. Elevations range from 125 to 300 mASL. The flat northern regions are characterized by large and extensive fens (ribbed, net and horizontal), leaving the area sensitive to flooding. Beach ridges, which mark former shore lines of glacial Lake McConnell, form linear islands in the wetland-dominated area and allow for scattered patches of mixed-wood and jack pine forests to grow.

2 ICING MAPPING METHODS

Icing distribution in the Yellowknife region was mapped with Landsat satellite imagery utilizing shortwave infrared (SWIR), near infrared (NIR), and visible (Blue, Green, Red) bands (wavelength regions) of the electromagnetic (EM) spectrum. The Thematic Mapper (TM) sensor (8-bit dynamic range) has been in orbit since 1984 on Landsat 5. The Enhanced Thematic Mapper Plus (ETM+) sensor (8-bit dynamic range), an advanced version of the TM sensor, is on board Landsat 7 which was launched in 1999, and Landsat 8 carries the Operational Land Imager (OLI) sensor with a 12-bit dynamic range. The band names, wavelength, and resolution of these three sensors are shown in Table 1, and a comparison of the Landsat 7 and 8 spectral bands is available at http://landsat.usgs.gov/L8_band_combos.php. Landsat scenes for WRS-2 path 49 and WRS-2 row 16 cover the study area, and the imagery was obtained from GLOVIS (http://glovis.usgs.gov/). The native projection of the imagery was Universal Transverse Mercator (UTM) zone 11 with WGS 84 as a

Table 1. Band designations for the Landsat satellites.

Band	Wavelength (micrometers)	Description	Resolution (m)
Landsat 5 Thematic Mapper (TM)			
1	0.45-0.52	Blue	30
2	0.52-0.60	Green	30
3	0.63-0.69	Red	30
4	0.76-0.90	Near Infrared (NIR)	30
5	1.55-1.75	Shortwave Infrared 1 (SWIR1)	30
6	10.40-12.50	Thermal Infrared	120
7	2.08-2.35	Shortwave Infrared 2 (SWIR2)	30
Landsat 7 Enhanced Thematic Mapper Plus (ETM+)			
1	0.45-0.52	Blue	30
2	0.52-0.60	Green	30
3	0.63-0.69	Red	30
4	0.77-0.90	Near Infrared (NIR)	30
5	1.55-1.75	Shortwave Infrared 1 (SWIR1)	30
6	10.40-12.50	Thermal Infrared	120
7	2.09-2.35	Shortwave Infrared 2 (SWIR2)	30
8	0.52-0.90	Panchromatic	15
Landsat 8 Operational Land Imager (OLI) and Thermal Infrared Sensor (TIRS)			
1	0.43-0.45	Coastal Aerosol	30
2	0.45-0.51	Blue	30
3	0.53-0.59	Green	30
4	0.64-0.67	Red	30
5	0.85-0.88	Near Infrared (NIR)	30
6	1.57-1.65	Shortwave Infrared 1 (SWIR1)	30
7	2.11-2.29	Shortwave Infrared 2 (SWIR2)	30
8	0.50-0.68	Panchromatic	15
9	1.36-1.38	Cirrus	30
10	10.60-11.19	Thermal Infrared 1 (TIRS1)	100
11	11.50-12.51	Thermal Infrared 2 (TIRS2)	100

datum. Icings are clearly visible in Landsat data following snowmelt (Harden *et al*., 1977; Hall and Roswell, 1981; Dean, 1984; Jeffries *et al*. 2005; Yoshikawa *et al*., 2007), so late-spring images were used (Table 2). However some data sets contained snow that had to be differentiated from ice. Images are prescreened in GLOVIS for cloud cover and scenes with less than 10% cloud cover were preferred. Higher cloud cover was accepted if the clouds were relatively transparent (more like haze), or if cloud-free data were available from the next satellite pass, or if data from another satellite in the Landsat constellation that could be used to fill in the covered area. The cloud cover requirements could not be met for all years, and consequently, not all years could be mapped (Table 2). There were also two years (2006 and 2011) when the only data available were Landsat 7 scenes acquired following failure of Scan Line Correction in the ETM+ instrument (SLC off). Following data acquisition, the ice mapping procedure consists of four main steps: preprocessing images, extracting ice, masking out water, and performing overlay operations in a GIS.

2.1 Image Preprocessing

All images used were level-one terrain-corrected products (L1T) with radiometric and geometric corrections, and free from sensor-, satellite-, and Earth-induced distortions. SLC-off images were processed as is; gap-filling techniques exist (*c.f.* Zhu *et al*., 2013), but because icings are ephemeral features, they could not be interpolated properly between scenes. All images were subsequently converted from digital number values (DN) to spectral radiance using sensor metadata provided along with the images, and were then converted to exoatmospheric reflectance (reflectance above the atmosphere) following Chander *et al*. (2009) (Figure 5a). Corrections for anisotropic reflectance variation due to topography and for the bidirectional reflectance distribution function were not applied to the limited study area in this demonstration study, but would be essential for mapping mountainous or large areas (Colby 1991).

2.2 Ice Extraction

Icing ice was mapped using three stages of image algebra. (Morse *et al.*, 2014). The approach capitalizes on the distinctly different reflectance and emittance of electromagnetic radiation between liquid water, solid water, and other materials.

Normalized Difference Snow Index (NDSI)

The NDSI is often used to discriminate between snow and ice versus soil, rocks, and cloud cover (Silverio and Jaquet, 2005; Hendriks and Pellikka, 2007). The index takes advantage of the exoatmospheric reflectance of snow and ice being high in the visible region of the EM spectrum and low in the SWIR1 region (Figure 5b), and is defined as the difference between the Green and the SWIR1 bands divided by their sum (Hall *et al*. 1995):

$$NDSI = [Green - SWIR1] / [Green + SWIR1]. \quad (1)$$

Figure 6a shows that the NDSI frequency distribution for the study area in the 2009 image (Figure 5c) was unimodal. Following Hall *et al*. (1995), 0.4 was selected as the threshold value for snow and ice (Figures 5d and 6a). However, because the images were acquired in late spring, they often include thawed or partially thawed water bodies; in this study region, many of those shallow lakes and ponds have a marl bottom or are turbid and, as a result, they are included in the snow and ice class. These features are problematic, because many of these lakes dry and become mud pans by midsummer and are not detected by a water discrimination index (as described below).

Table 2. Landsat image acquisition dates, IDs, satellite number, cloud cover, and Scan Line Correction turned off (L7 SLC-off).

Year	Acquisition Date	Landsat Image ID	Landsat #	Cloud Cover (%)	L7 SLC-off
1984	21-May-84	LT50490161984142	5	0	
1985	28-Aug-85	LT50490161985240	5	0	
1991	10-Jun-91	LT50490161991161	5	13	
1992	28-Jun-92	LT50490161992180	5	3	
1993	15-Jun-93	LT50490161993166	5	0	
1994	02-Jun-94	LT50490161994153	5	0	
1996	23-June-96	LT50490161996175	5	0	
1998	12-May-98	LT50490161998132	5	0	
1999	16-Jun-99	LT50490161999167	5	1	
2000	10-June-00	LE70490162000130	7	3	
2001	12-May-01	LE70490162001132	7	8	
2002	02-Jul-02	LE70490162002183	7	37	
2004	13-Jun-04	LT50490162004165	5	0	
2005	31-May-05	LT50490162005151	5	0	
2006	11-June-06	LE70490162006162	7	0	Yes
2008	23-May-08	LT50490162008144	5	19	
2009	11-June-09	LT50490162009162	5	0	
2010	29-May-10	LT50490162010149	5	0	
2011	24-May-11	LE70490162011144	7	0	Yes
2013	21-May-13	LC80490162013141	8	2	
2014	09-June-14	LC80490162014160	8	9	
2015	27-May-15	LC80490162015147	8	0	

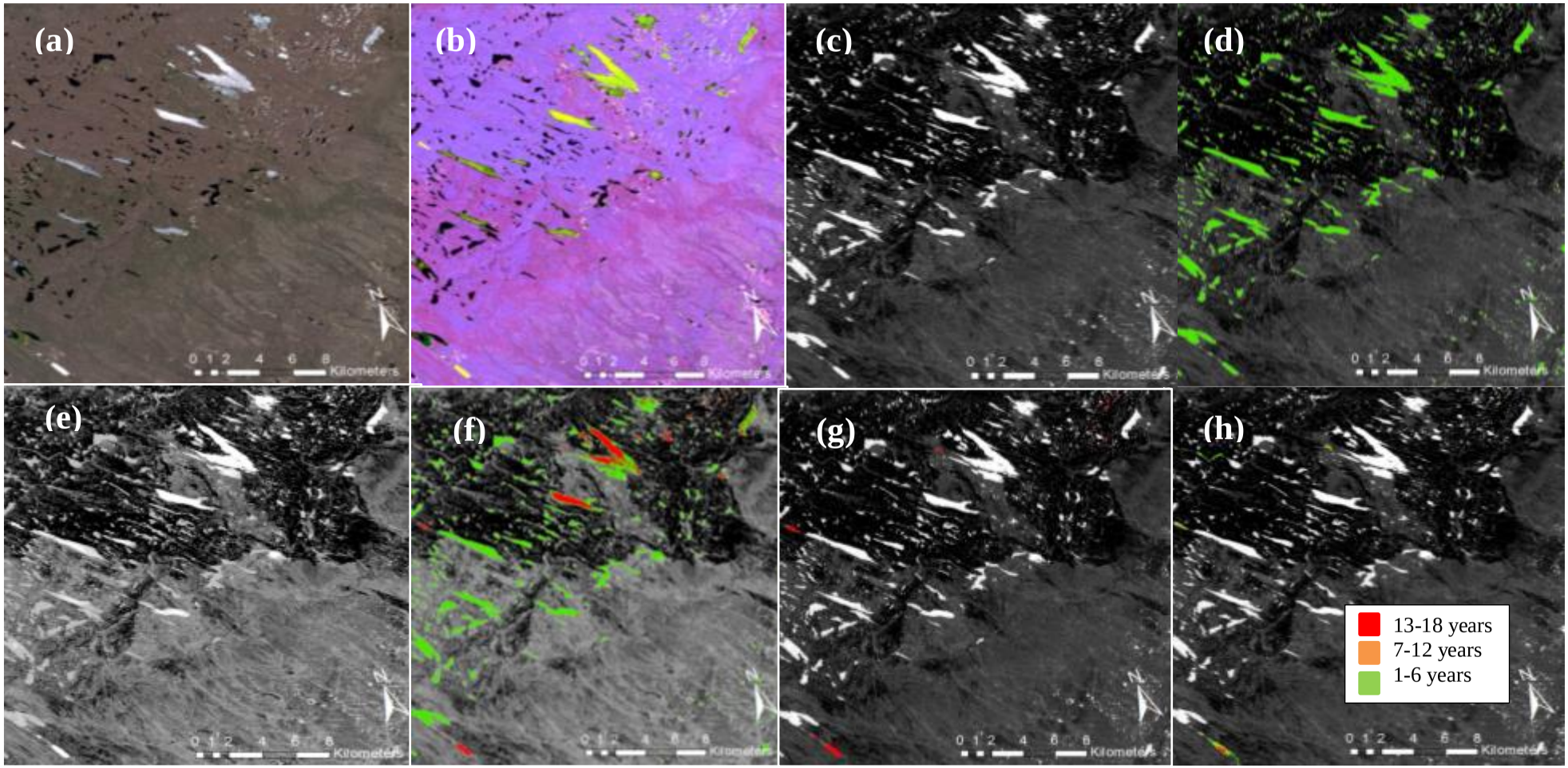

Figure 5. Processing stages shown for a subset of the 2009 Landsat 7 data: (a) True colour composite (Red:Red, Green:Green, Blue:Blue); (b) False colour composite (Red:NIR, G:Green, Blue:SWIR1) (c) Normalized Difference Snow Index (NDSI); (d) Extracted ice and snow shown in green colour; (e) Maximum Difference Ice Index (MDII); (f) Extracted ice shown in red colour with snow in green; (g) Icings remain after lake and river ice are removed with a water mask; and (h) Cumulative icing occurrence over 24 years with red, orange and green indicating a return frequency of 13-18 years, 7-12 years, and 1-6 years, respectively.

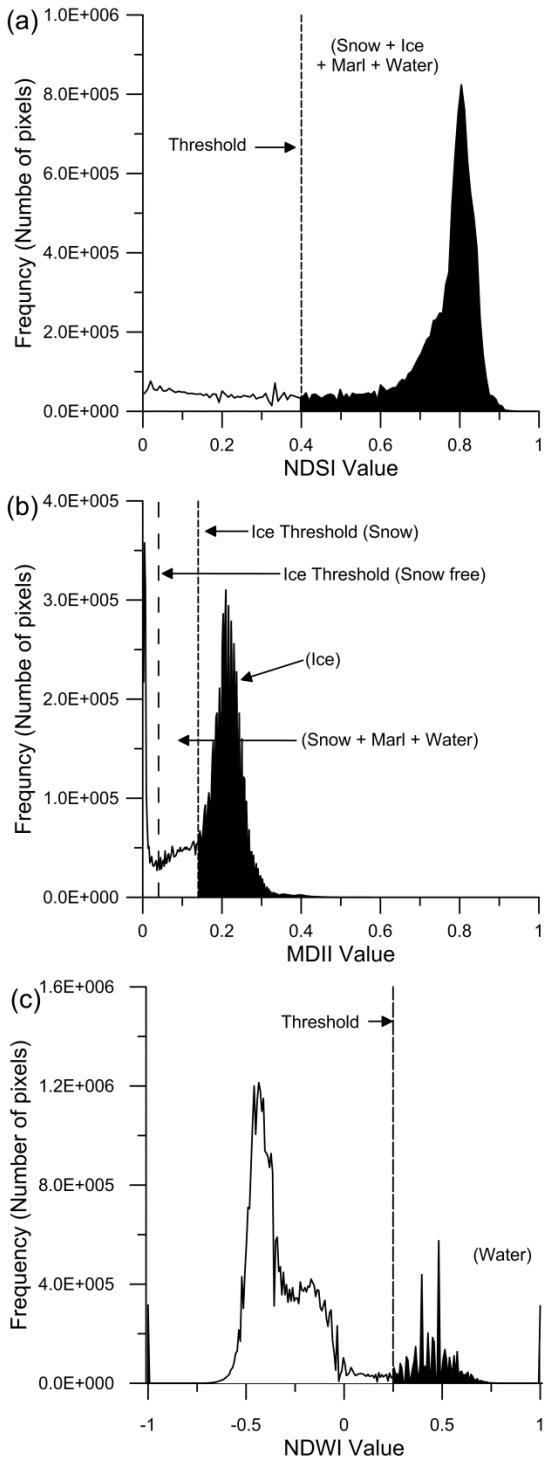

Figure 6. Frequency distributions showing: (a) NDSI unimodal character related to snow, ice, marl and water; (b) MDII compressed bimodal character related higher contrast between ice versus snow, marl and water; and (c) NDWI bimodal character related to higher contrast between water vs land and clouds.

Maximized Difference Ice Index (MDII)

Although the images are ideally snow-free, there is a gradual southwest to northeast increase in elevation across the scene from about 160 to 450 mASL and, consequently, some images may have snow at elevated locations (Figure 5). In addition, the NDSI values above threshold may include shallow ephemeral marl basins and water (NDSI is designed for frozen landscapes where wet surfaces are not typically a problem). Thus the second step is to differentiate between ice, snow, wet marl and water. Keshri *et al*. (2009) proposed following the NDSI with a Normalized Difference Glacier Index (NDGI) to separate snow and ice from an ice and debris mix. However this index was not employed because it produced a unimodal distribution when tested with images that included snow or shallow lakes and debris would be unusual on an icing. We found that a basic difference index between Green and SWIR1 created a bimodal distribution that differentiated between snow and ice (Figure 6b). The contrast of this bimodal distribution is exaggerated by multiplying the difference between the Green and the SWIR1 bands by their sum in a proposed Maximum Difference Ice Index (MDII) that was used as the second stage (Figure 5e):

$$MDII = [Green - SWIR1] \times [Green + SWIR1] = [Green^2 - SWIR1^2]. \quad (2)$$

MDII values are determined for pixels within the thresholded range of NDSI values, thus the spatial extent of MDII is restricted by NDSI. Therefore, atmospheric effects related to the use of an "unnormalized" difference index (MDII) are likely minimal, as the snow and ice pixels assessed are already defined by the NDSI. From visual comparison of MDII results with color composite images of Landsat scenes (5, 7, or 8) with snow cover, we established that a MDII threshold of 0.144 discriminates ice from snow, wet marl, and water (Figure 3c). In snow-free scenes a threshold value of 0.040 may be used. Extracted icing data were saved in two Boolean classes with 1 for ice and 0 for non-ice.

2.3 Water Masking

The delineated ice will also include any river and lake ice present. Consequently, a water mask must be applied to remove river and lake ice and leave only land-fast ice. Water features may be discriminated in Landsat images with a Normalized Difference Water Index (NDWI) determined from exoatmospheric reflectance following McFeeters (1996):

$$NDWI = [Green - NIR] / [Green + NIR], \quad (3)$$

where water is indicated by values greater than a threshold of 0.25 in order to separate water from cloud shadow (Figure 6c). Since water levels fluctuate from year to year, or over a season, a maximum water mask was created by combining NDWI results from summer images from different years (Table 3). Water level data from stream gauges were used to aid selection of "high water" years to reduce the number of images required for this purpose (Water Survey of Canada, 2016). The Water Survey of Canada's historical hydrometric data for station 07TA001 or "La Martre River below outlet of Lac la Martre" was used. For comparison, station 07SB010 or "Cameron River", was also analyzed to confirm years with high water levels (Figure 7). Water level data were only available for the year 2001 and onward, therefore prior to this date, annual precipitation from the Yellowknife Airport was used. Once summer images were combined, the water mask was expanded outward by 60 m (2 times the pixel size) in order to eliminate substantial snow and ice that might accumulate along shorelines and remain past the nominal snowmelt period due to non-icing processes. Application of the water

Table 3. Landsat image acquisition dates, IDs, satellite number and cloud cover for water masking.

Year	Acquisition Date	Landsat Image ID	Landsat #	Cloud Cover (%)
1985	August 28, 1985	LT50490161985240	5	0
1991	June 10, 1991	LT50490161991161	5	19
1992	June 28, 1992	LT50490161992180	5	7
1997	July 28, 1997	LT50490161997209	5	2
1999	August 3, 1999	LT50490161999215	5	4
2005	August 3, 2005	LT50490162005215	5	1
2006	July 5, 2006	LT50490162006186	5	12
2009	August 30, 2009	LT50490162009242	5	1
2013	July 24, 2013	LC80490162013205	8	0

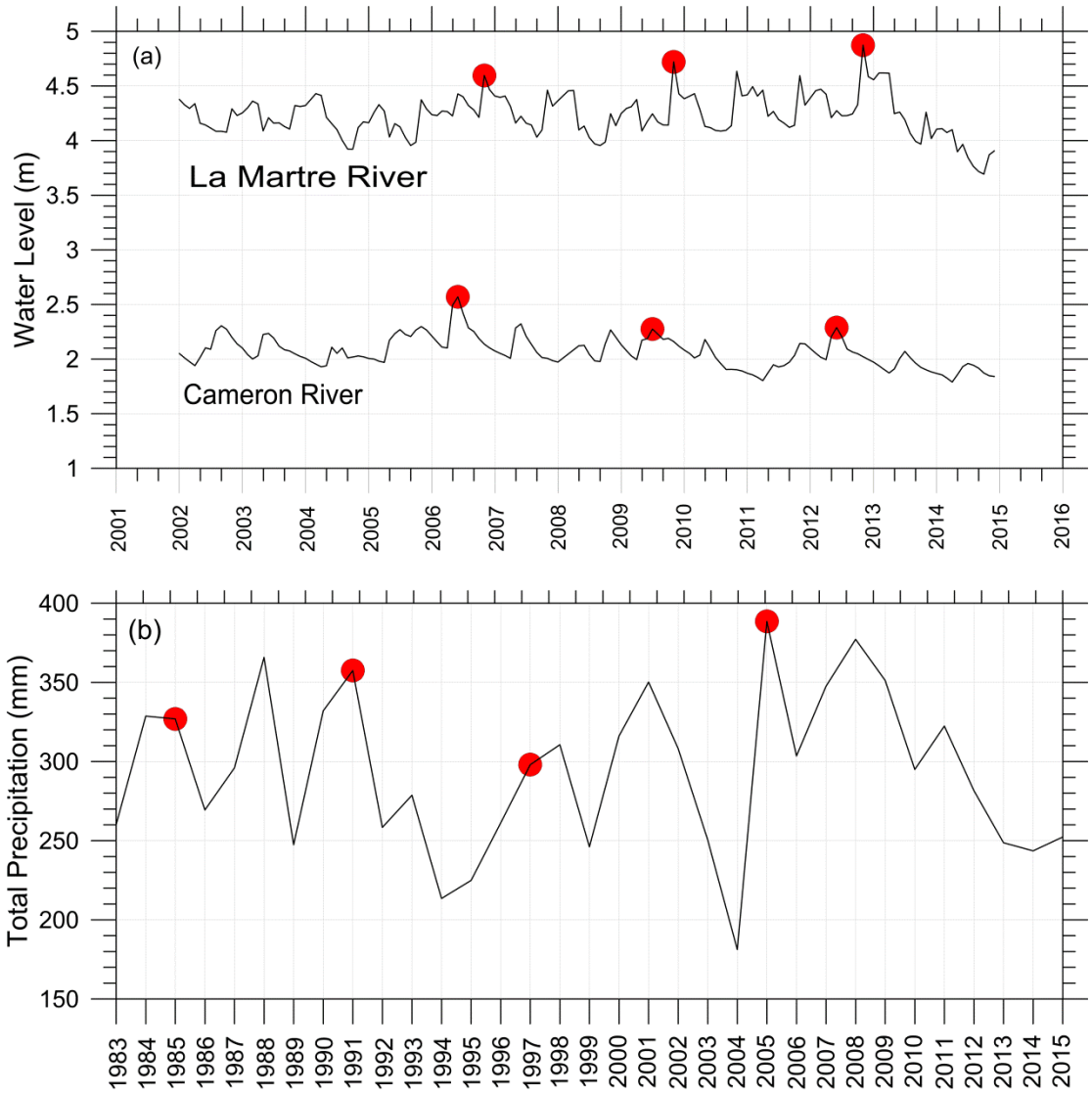

Figure 7. (a) Water levels measured from la Martre River below outlet of Lac la Martre (Water Survey of Canada station 07TA001), Northwest Territories and from Cameron River (Water Survey of Canada station 07SB010), Northwest Territories. (b) Total precipitation from historic climate data at Yellowknife Airport, Northwest Territories. Red circles indicate years utilized for water masking.

mask (Figure 5f) to the icing data in a GIS ensures that the only ice bodies mapped are land-based icings (Figure 5g).

2.4 Post-processing Overlay Analysis

Once the icings for a particular year were mapped, the raster layer was imported to a GIS and the icings were extracted to polygons that retained the pixel edges (no smoothing). This allowed area calculations to reflect the pixel count, and future overlay operations in a GIS to reflect pixel activity. Any polygon with a value of 0 (non-ice) was deleted, and the areas of the remaining polygons were calculated. A new polygon attribute was added to indicate the year. Once all raster layers were extracted, a visual comparison of the mapped icings and the corresponding false colour composite image identified areas that required further processing. In some instances, the threshold values for MDII were changed in order to correct for snow that was incorrectly mapped as icings. Clouds that were classified as icings were manually deleted. The northwest (LGULS) and the south (HSLS) ecoregions of the study area displayed reoccurring snow drifts due to high local relief and these were manually deleted.

In order to determine the cumulative icing occurrence and interannual dynamics of icings (eg. Figure 5h), the icing data for each year were combined in a GIS by computing their geometric union. Though the Landsat images are all from WRS-2 Path 49 / Row 16, there was some variation in the spatial extent of each scene. Therefore, the data were clipped to the maximum extent of the overlap region. The area of each unique polygon (following the geometric union) was then calculated. In order to isolate land-based ice, the expanded water mask raster layer was extracted to a polygon shapefile and erased from the clipped data layer. The non-expanded water mask raster layer was also erased from a clipped layer of the ecoregions, in order to ensure that all the ecoregion area used in further analysis was terrestrial so as to normalize icing density for ecoregions that contained large bodies of water.

As it was common for icing such as those on rivers to appear as multiple polygons due to the water masking, and because the extent of an icing at a particular location varies from year to year, a new attribute was added called “Aggregation ID”; icing polygons within 45 m (1.5 pixels) of one another in the same year were considered to be from the same icing and were assigned the same Aggregation ID. A practical minimum aggregate icing size of 2 pixels (1800 m^2) was set as a threshold, and smaller polygons were deleted. A GIS overlay was used to spatially relate the Aggregation ID to the icings, and total icing counts were determined by the number of different aggregation IDs and therefore icings.

The polygon attributes from each year of mapping were then used to determine metrics such as the annual icing area or the total icing area for a particular icing over the total number of years. The icing activity (return frequency) of a particular location was determined from the count of instances (years) when ice was present at the pixel. A further GIS overlay operation assigned the ecoregion where the icing occurred as an additional attribute, which allowed for an assessment of the regional distribution of icings.

3 RESULTS AND DISCUSSION

A three-step sequential classification process using the NDSI, MDII, and a NDWI was used to map icings in the study region (Figure 8)The final map of total icing distribution is shown in Figure 4.

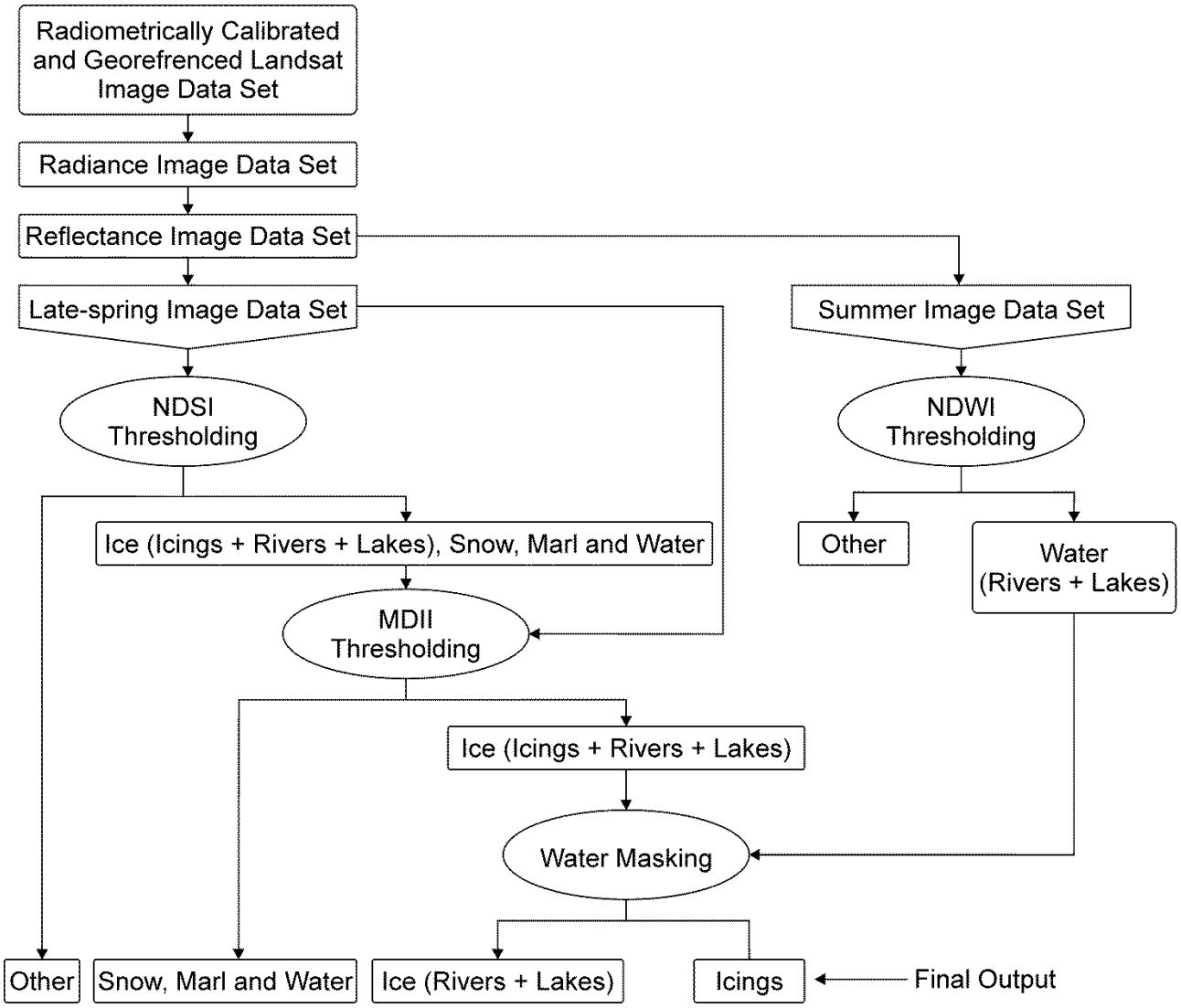

Figure 8. Workflow diagram for the three-step sequential discrimination of icings from snow, river and lake ice, and other surfaces using Landsat data.

A quantitative assessment against an independent measurement of icing area such as aerial photography is difficult, because aerial photographs of the region are taken in summer to coincide with peak vegetation greenness. Consequently each year's icing mapping result was assessed visually; The results were overlaid on the true color composite of the image data where the icings are visually distinguishable from shallow marl ponds and, as a consequence of the applied MDII threshold values, none of these ponds were classified as ice. In order to visually assess the discrimination between snow and ice classes, the mapping results were overlaid on a summer image to ensure that the icing class data were located in a drainage area (*i.e.* stream valleys or floodplains). There were only a few instances where they were not, and it was sufficient to manually delete them. However, due to the MDII threshold values, icings are likely underestimated and snow is overestimated. This does not imply that snow-free images taken later can improve the overall results, because though a lower MDII threshold can be applied to map ice in such images, the increased time for ablation means that smaller icings may have disappeared and the margins of larger icings have likely retreated. It is emphasized that because of icing dynamics, and because of the timing of image acquisition each spring, the relative number and area of icings is likely more important to this case study than absolute values between years and ecozones. However, future work could include acquiring supplementary remotely sensed data that would enable a more robust accuracy assessment.

Locations of high visible reflectance besides those with snow and ice, such as beaches or active dune fields, were not problematic because of low surface moisture. The only non-icing features that were classified by the method used in this study were high, cold clouds containing ice and these instances were manually deleted. A cloud mask could be generated, but cloud detection techniques commonly mistake snow and ice for cloud (Zhu and Woodcock, 2012). Alternatively, a cloud shadow-matching approach could be explored (Choi and Bindschadler, 2004).

3.1 Icing Distribution and Interannual Variation

Satellite image date and cloud cover had little influence on variations of the total icing area for the 22 years investigated (Figure 9). Spatial gaps due to "SLC-off" image data likely affected the results for 2006 and 2011, however, the gaps cover only 22% of the image, icings are well distributed (Figure 4), and the results from those two years are not examined in isolation. Therefore, the relative quantities determined for those years are considered acceptable for the current demonstration and were included.

Overall, the cumulative extent of icings covered 2.15 km^2 of land, or about 0.0068% of the land in the study area (31545.36 km^2). However, physiography controls the occurrence of icings (Morse *et al*., 2015), and consequently the spatial and temporal variations of icings is related to ecoregion (Figures 4, 10, 11, 12 and 13). It is also clear that icing activity is related to meteorological conditions; however, local meteorological parameters may not explain all interannual variation of icing extent, as ground water sources may be influenced by differing meteorological conditions some distance away from the spring (Hall and Roswell, 1981; Kane *et al*., 2013). As a consequence of variable meteorological conditions, interannual variation of icing area was not coincident amongst ecoregions (Figure 10).

Lac Grandin Upland Low Subarctic

The highest overall total icing density (0.0023 km^2 km^{-2}) and area (0.93 km^2) of any ecoregion over the 22 years examined occurred at LGULS (409.53 km^2) (Figure 10), where slope fens, northern ribbed fens, and spring fens are widespread along the lower slope positions. Icings develop in stream valleys and in the vicinity of springs that feed the numerous fens (Ecosystem Classification Group, 2007). The high density can be attributed mainly to a high regional icing count (40), and extensive icing development in 1984 (0.33 km^2), 1993 (0.36 km^2), 2004 (0.49 km^2), 2008 (0.45 km^2) and 2013 (0.48 km^2) (Figure 11), as the ecoregion covers a relatively small area. Annual icing area was as low

as 0 km^2 (Figure 11), with a 0.22 km^2 median annual area. Many icings are relatively frequent and large, with icings active 50% of the time or more cumulatively constituting about 17% of the total icing area (Figure 14b). The largest icing within the study region (0.53 km^2) constitutes about half of the total icing area and is found partly in this ecoregion.

Lac Grandin Plain Low Subarctic

The icing area (0.45 km^2) of the LGPLS ecoregion (5119.57 km^2) over the 22 years is relatively large and second only to the LGULS ecoregion (Figure 10), while it has the highest regional icing count (46). Icing development is concentrated in the fluted terrain along the western slopes of the ecoregion, where limestone and dolomite bedrock with karst topography is widespread and icings develop in the vicinity of springs that feed the numerous marl ponds (Ecosystem Classification Group, 2007). In contrast to the LGULS ecoregion, the overall icing density is low (0.000088 km^2 km^{-2}) and can be attributed to the comparatively large area of the ecoregion. The most active icings re-develop in 14 of the 22 years, and about 50% of the cumulative icing area is active; the remainder consists of icings occurring for only one year (Figure 14b). The most extensive icing occurred in 2008 and covered 0.15 km^2 (Figure 11). Much of this area's icing coverage can be attributed to the largest icing of the study area that extended from the LGULS into the LGPLS ecoregions, with the most active areas of the icing residing in LGULS and only the infrequent icing development extending into the LGPLS.

Bulmer Plain Low Subarctic

The lowest icing density (3.6 $x10^{-6}$ km^2 km^{-2}) of any ecoregion occurred in the BPLS (9003.52 km^2) where the flat terrain is riddled with marl ponds (Ecosystem Classification Group, 2007). A relatively low count of icings (11) with low total icing area (0.0324 km^2), combined with the largest ecoregion area account for the low density (Figure 10). Maximum icing return frequency is only 22% and this accounts for about 8% of the icing area (Figure 14b). Annual icing area ranges from nil to 0.009 km^2 (Figure 11).

Great Slave Lowland High Boreal

GSLHB (990.1 km^2) displayed the second lowest number of icings (4) and lowest total icing area (0.014 km^2) of any ecoregion (Figure 10). Extensive infilling with fined-grained sediments between outcrops and in bedrock fractures may limit the extent to which springs and thus icings can occur. (Ecosystem Classification Group, 2008). Each icing developed only once (Figure 14a). The most extensive icing occurred in 2011 and covered 0.0243 km^2 (Figure 11), but most icings were small, leading to a median annual area of 0 km^2.

Great Slave Upland High Boreal

GSUHB (280.19 km^2) has a moderate number of icings (13) and a total icing area of 0.079 km^2, yielding a density of 0.00028 km^2 km^{-2} (Figure 10), which is second only to LGULS. Sediment deposits in rock fractures and between outcrops are thin and much more discontinuous than at GSLHB (Ecosystem Classification Group, 2008) and icings are more likely to develop. Annual icing areas ranged from a minimum of 0.0009 km^2 to 0.0072 km^2 (Figure 11), with a 0 km^2 median. Icing return frequencies are up to 32% with nearly 2% of the icing area active 25% of the time (Figure 14b), which is much more than the adjacent GSLHB ecoregion.

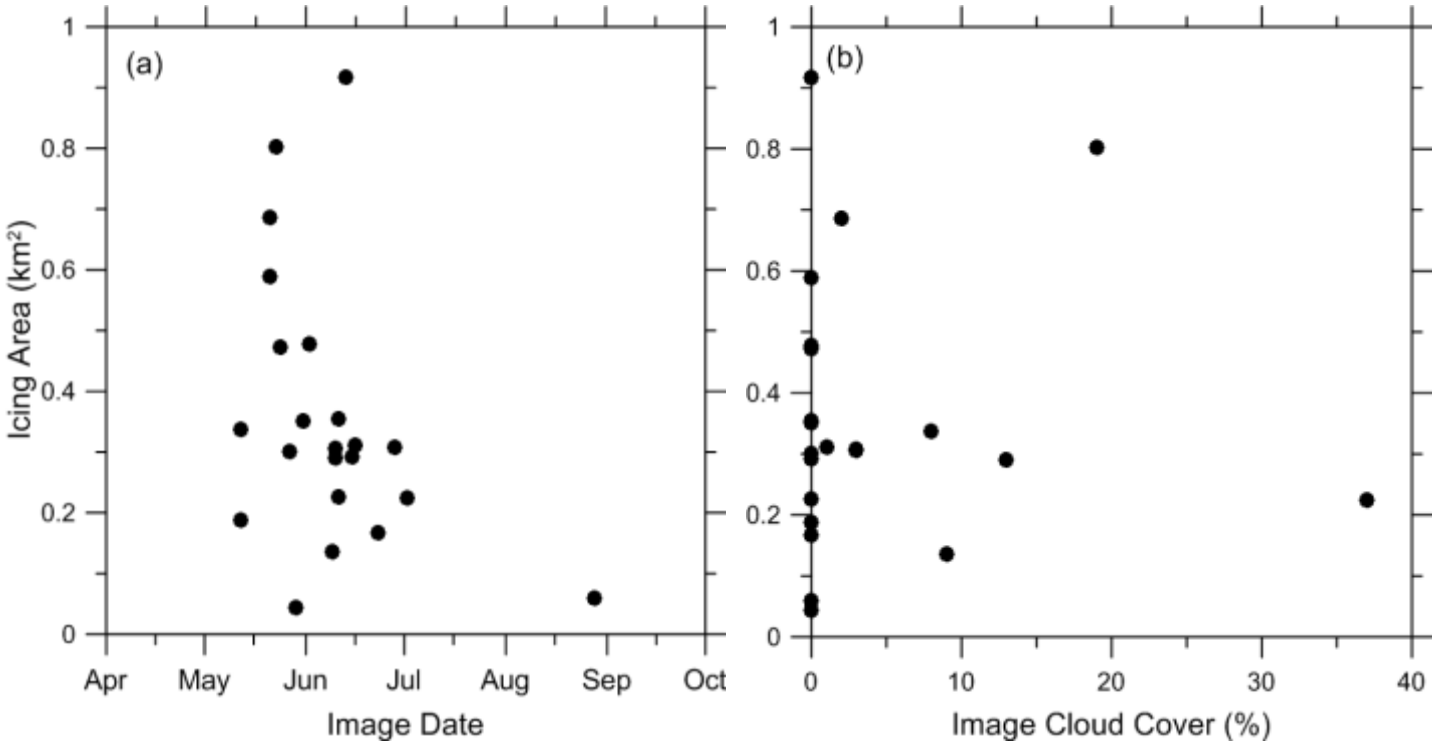

Figure 9. Total icing area versus (a) image acquisition date and (b) percent cloud cover for years mapped (22 years).

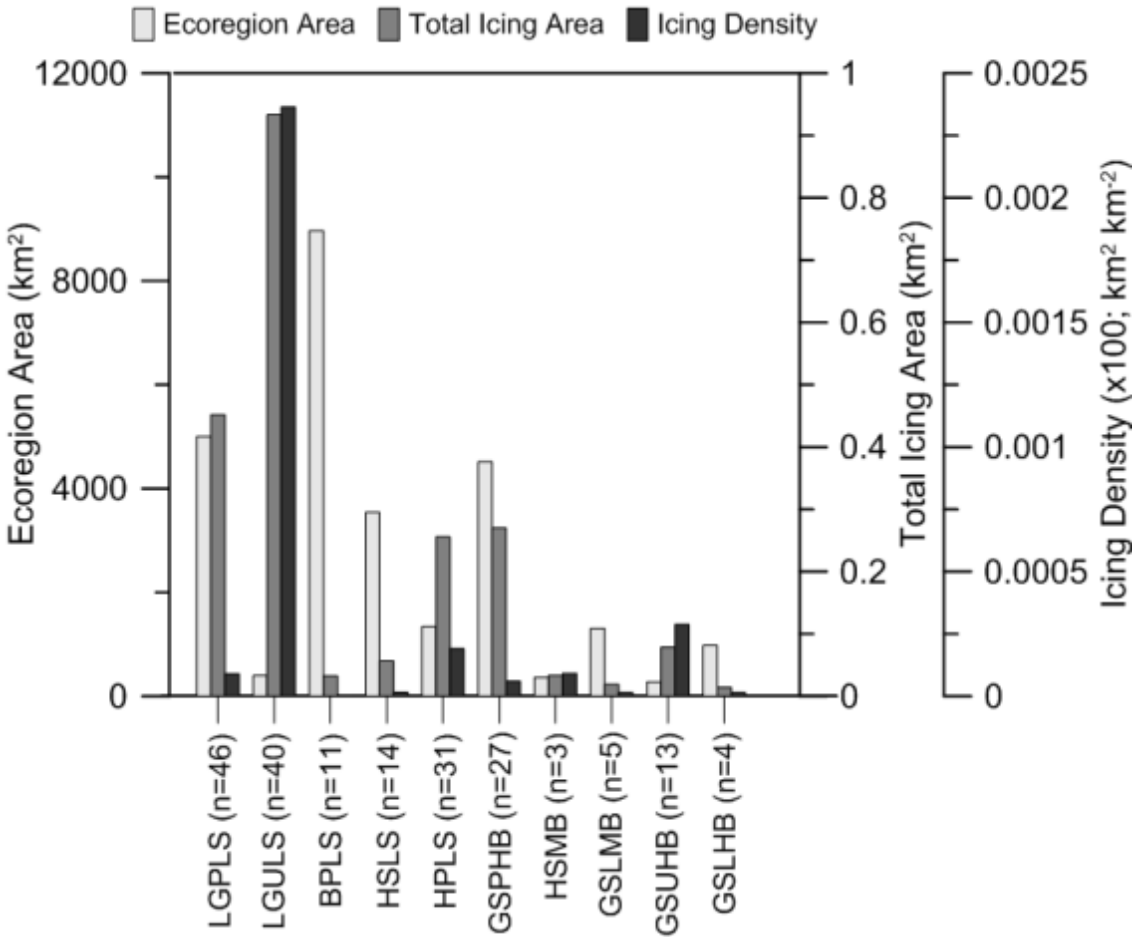

Figure 10. Regional area, total icing area, and total icing density determined for ecoregions in the Yellowknife area. Lac Grandin Plain Low Subarctic (LGPLS), Lac Grandin Upland Low Subarctic (LGULS), Bulmer Plain Low Subarctic (BPLS), Horn Slopes Low Subarctic (HSLS), Horn Plain Low Subarctic (HPLS), Great Slave Plain High Boreal (GSPHB), Horn Slopes Mid Boreal (HSMB), Great Slave Lake Mid Boreal (GSLMB), Great Slave Upland High Boreal (GSUHB), and Great Slave Lowland High Boreal (GSLHB).

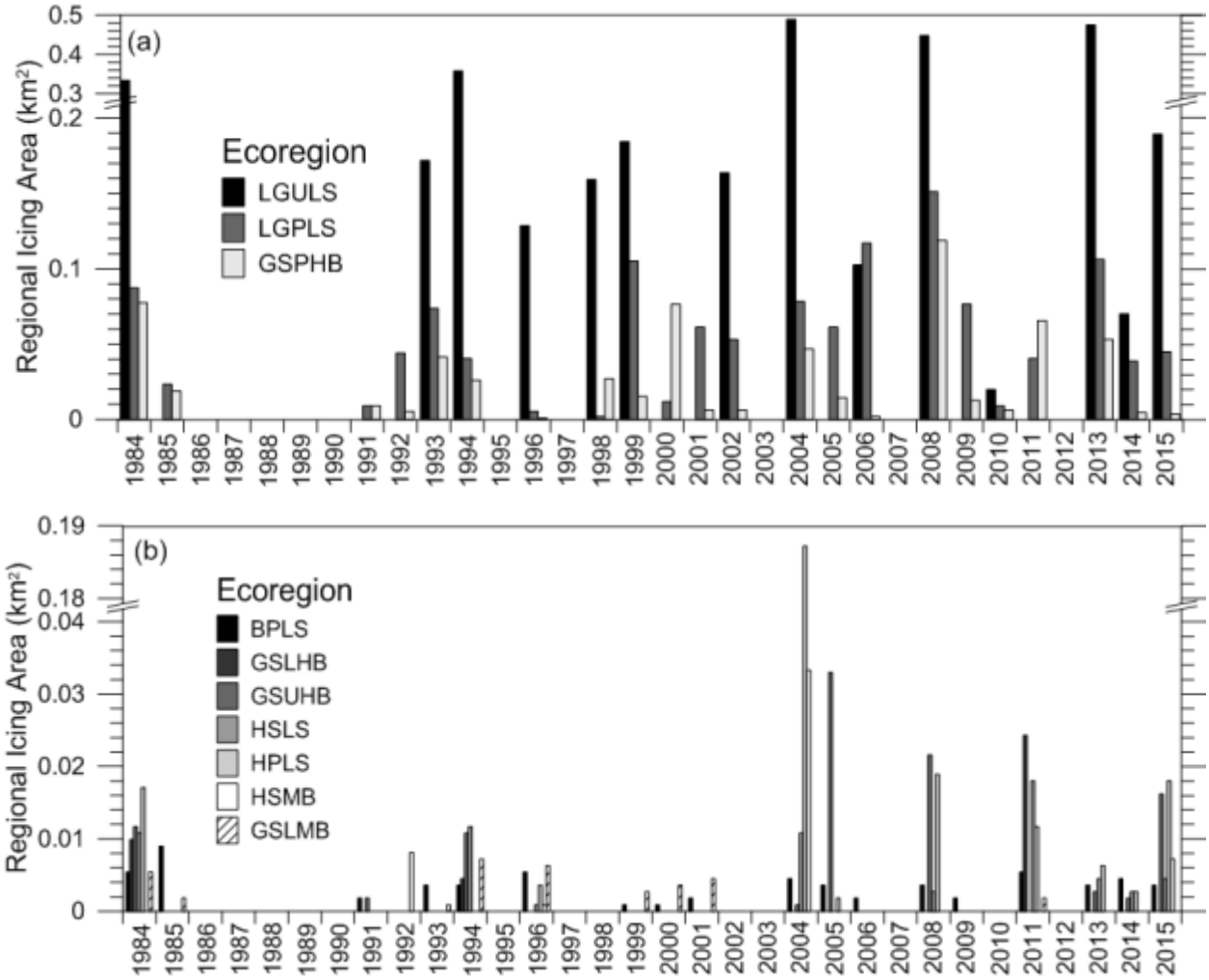

Figure 11. Annual icing area (1984-2015) for ecoregions in the study region with (a) relatively large icing areas, and(b) relatively low icing areas. Lac Grandin Plain Low Subarctic (LGPLS), Lac Grandin Upland Low Subarctic (LGULS), Great Slave Plain High Boreal (GSPHB), Bulmer Plain Low Subarctic (BPLS), Horn Slopes Low Subarctic (HSLS), Horn Slopes Mid Boreal (HSMB), Great Slave Lowlands Mid Boreal (GSLMB), Great Slave Upland High Boreal (GSUHB), Great Slave Lowland High Boreal (GSLHB), Horn Plateau Low Subarctic (HPLS)

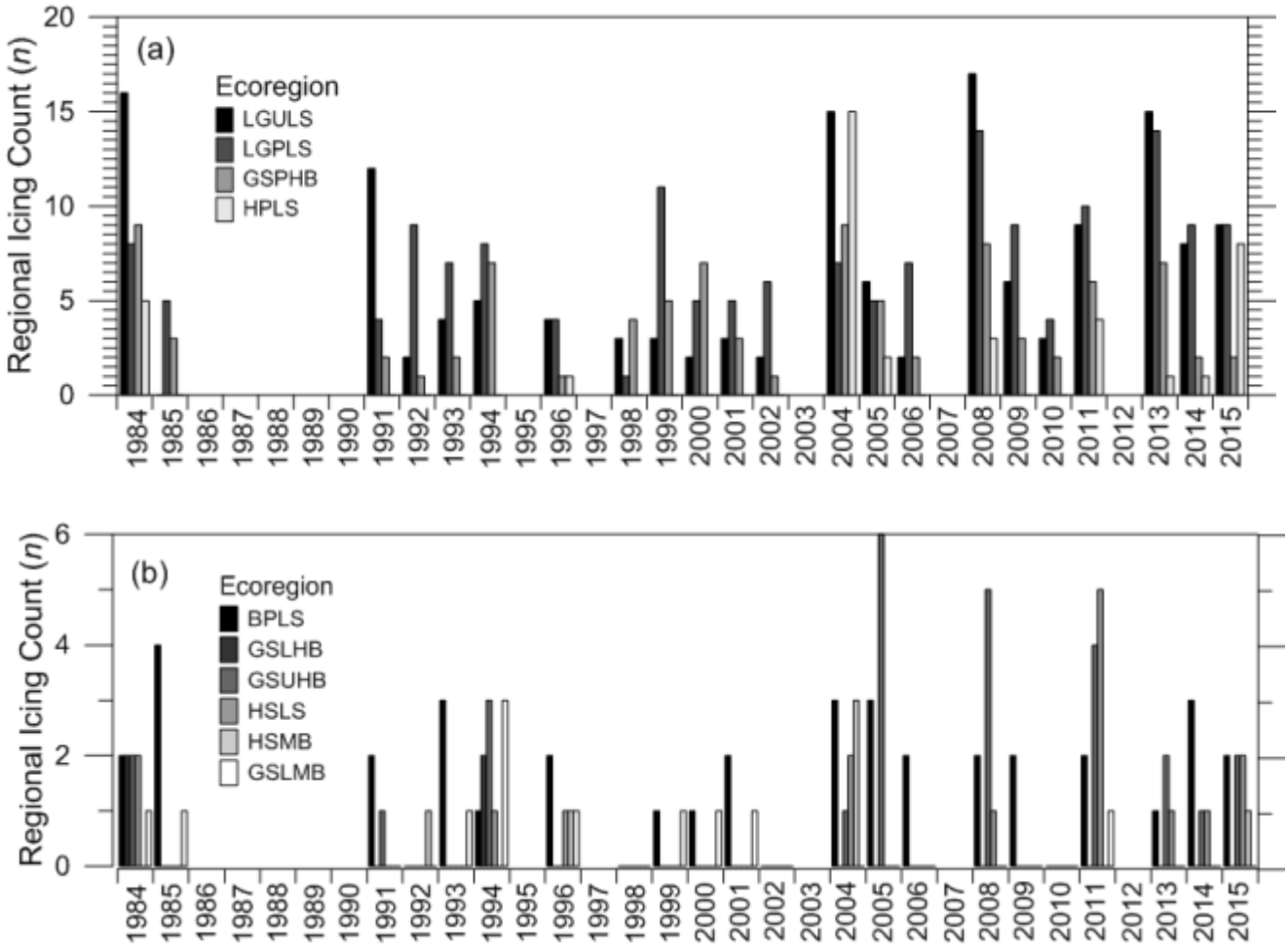

Figure 12. Annual icing counts for ecoregions displaying relatively(a) high and (b) low values.

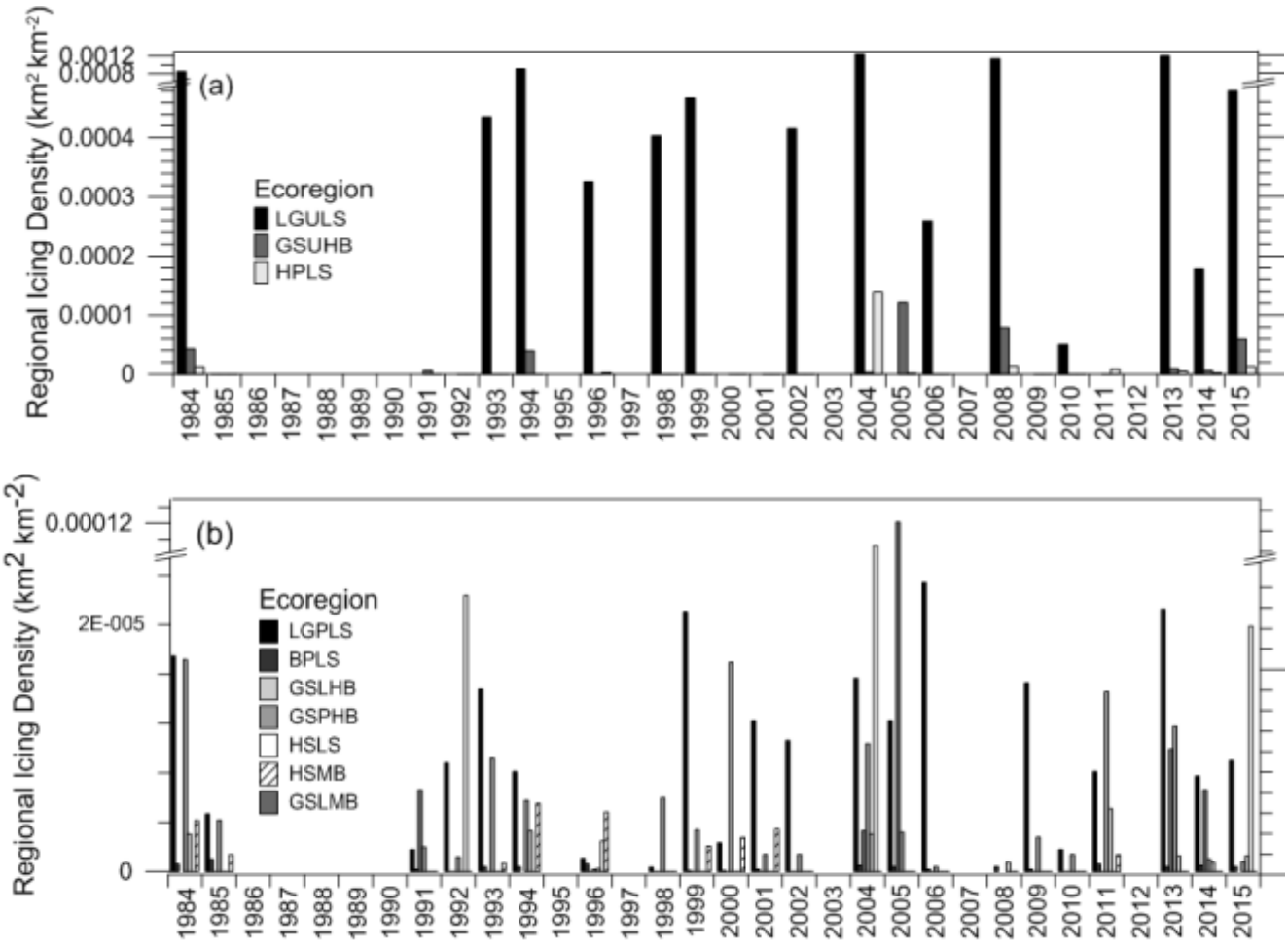

Figure 13. Annual icing area normalized by ecoregion area for ecoregions with icing densities that are relatively (a) high and (b) low.

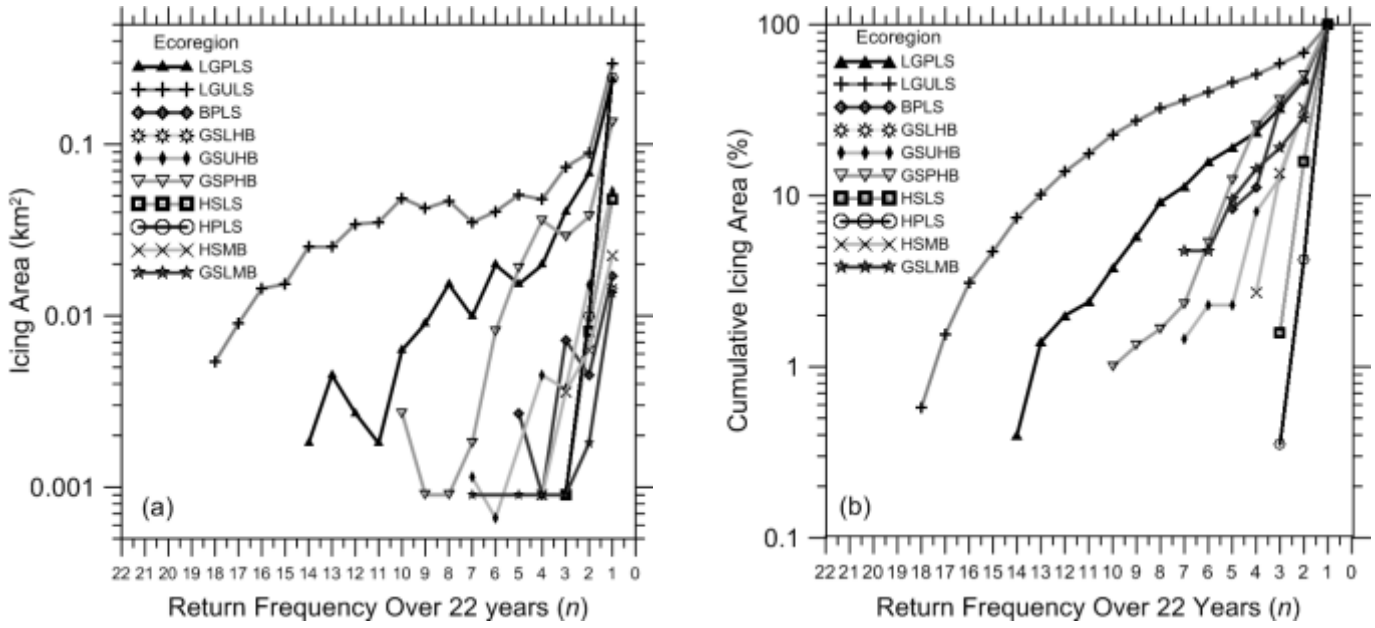

Figure 14. Icing dynamics in the Yellowknife area determined from 22 late-spring Landsat images: (a) icing size-frequency distribution, and (b) cumulative icing area versus icing return frequency

Great Slave Plain High Boreal

GSPHB (4452.40 km^2) has a total icing count (27) and icing area (0.27 km^2) higher than the adjacent GSUHB ecoregion due to widespread limestone and dolomite bedrock with karst topography, which allow icings to develop in the vicinity of springs that feed some of the numerous marls ponds (Ecosystem Classification Group, 2007) (Figure 10). The relatively flat terrain of the uplands allows icings to potentially develop over more extensive areas, as overflow is not as restricted as it is within a valley. The low density can be attributed to a significantly large ecoregion. Annual icing area ranged from 0.0009 km^2 to 0.12 km^2 with a median of 0.015 km^2. Many icings returned relatively frequently, some up to 10 times (Figure 14a). Icings that were active for more than one year had areas of 0.004 km^2 or less (Figure 14a), which cumulatively constitute 50% of the total icing area (Figure 14b).

Horn Slopes Low Subarctic

The HSLS (3543.79 km^2) ecoregion has a count of 14 icings, (0.057 km^2), with icing development most likely to occur along gentle northern slope stream channels where there is seepage from the HPLS (Ecosystem Classification Group, 2007) (Figure 10). Icings are small, with icing areas ranging from 0.0009 km^2 to 0.018 km^2, with a median of 0 km^2. Return frequency is low, with the most active icings only returning 13.6% of the years (Figure 14a) and contributing to only 1.6% of the cumulative icing area (Figure 14b).

Horn Plateau Low Subarctic

The most southerly of the ecoregions, the HPLS (1278.54 km^2), has a total icing area of 0.27 km^2 and a density of 0.0002 km^2 km^{-2}, making it one of the densest ecoregions because of its small area and high number of icings (31) (Figure 10). Most of the icing area can be attributed to extensive icing development in 1984 (0.17 km^2), 2004 (0.19 km^2), 2008 (0.019 km^2), and 2015 (0.018 km^2) (Figure 11) along the same river channel in the south-west of the ecoregion. Icing development in this ecoregion is infrequent, with the most active icings only developing 3 times (Figure 14).

Horn Slopes Mid Boreal

The smallest ecoregion within the study area, HSMB (334.74 km^2), has a correspondingly low regional icing count (3), icing area (0.033 km^2) and density (0.0001 km^2 km^{-2}) (Figure 10). The icings present in this study area are mainly icings that have extended from, or are peripheral to, the HPLS. These icings are small and infrequent (Figure 14). The ecoregion extends far beyond the study area where fens and ground seepage are common (Ecosystem Classification Group, 2007), potentially indicating icings further south.

Great Slave Lowland Mid Boreal

The most southeastern portion of the map encompasses a portion of GSLMB (1261.42 km^2), a large ecoregion that extends much further beyond the study region to the southeast. It has a low regional icing count (5), icing area (0.019 km^2), and correspondingly low regional icing density (0.000015 km^2 km^{-2}) (Figure 10). Annual icing area ranged from 0.0009 km^2 to 0.054 km^2 with a median of 0 km^2, indicating that icings were small. Icings mostly develop in the northern, ribbed fen area of the ecoregion (Ecosystem Classification Group, 2007), and 5% of cumulative icing area returns for seven years (Figure 14).

4 SUMMARY AND CONCLUSIONS

Nearly 200 icings were mapped from 22 late-spring Landsat images of the region around Whati (31545 km^2) (Figure 4). Size frequency distribution curves, derived from counts of instances when ice was present at a pixel, indicate that icing area is inversely related to return frequency (Figure 14). That is, the vast majority of icing ice reoccurs 10 years or less. Icings varied substantially between

ecoregions, with the largest and most numerous occurring at LGULS, and the least numerous at GSLHB. The limestone and dolomite bedrock terrain at LGULS likely promotes the development of numerous icings via karst drainage networks. At GSLHB, the granite bedrock is capped by thick unconsolidated deposits with permafrost that may limit emergence of springs at the surface and significantly affect groundwater recharge pathways. Icings at GSUHB are numerous and well-spaced for a small ecoregion area and, consequently, this region has a significant icing density, second only to LGULS (Figure 13); the next highest icing density was found in the HPLS. The high icing densities at LGULS, GSUHB, and HPLS are all associated with relatively high elevations, as they are all classified as "upland" or "plateau". The ecosystems classified as "plains"—LGPLS, BPLS, and GSPHB—displayed varying regional icing densities, areas and counts. LGPLS and GSPHB had significant icing activity due to exposed karst topography throughout the region. The BPLS ecoregion, while having similar underlying bedrock, does not display surface expression of karst, is capped with more unconsolidated sediments, and has much lower icing activity. The slope ecoregions—HSLS and HSMB—displayed low regional icing areas, counts, densities, and frequencies, with the most active icing reoccurring in only 4 out of 22 years (Figure 14). While there are springs that occur in these ecoregions where ground water moves towards the plains and lowlands, the dynamic landscape and underlying shale bedrock were relatively non-conducive to icing development. Finally, the GSLMB, another lowland in the study area, displayed very low icing areas, count, and a density only slightly higher than the GSLHB (Figure 10).

Icing area and count varied considerably from year to year (Figure 10, 11, 12, 13 and 14), and icing areas were not coincident each year, suggesting differences in climate regimes between ecoregions affected factors such as rainfall and winter warming events that are important in the Great Slave Region (Morse *et al*. 2015). Variations in snow cover may also affect icing occurrence and distribution in the region. In addition, the distance to groundwater sources likely varies among the ecoregions, such that icings is some regions may also be influenced by meteorological conditions outside of the study region.

This study area displayed less icing activity overall than what was mapped in the adjacent study area by Morse et. al., (2014), which encompasses the Great Slave Region and is centred approximately on Yellowknife. Total icing count, area and density were all much higher in that study, and nearly 5,500 icings were mapped, with a cumulative extent of 86 km^2 or about 0.39% of the land in the study area. However, similar to the findings of this report, icing area was inversely related to return frequency as Morse et al., (2014) found 90% of icing area had a return period of 10 years or less out of a total of 24 years.

Icing occurrence and reoccurrence maps provide important geoscience information required for development and transportation infrastructure planning. This report presents an icing occurrence and reoccurrence map for Lac la Martre area, NWT. These data, generated using a maximum difference band ratio approach, provide the first assessment of icing distribution in this area. This preliminary information is required to assess terrain risks to northern transportation infrastructure, and may guide route selection for future transportation corridors within the region.

5 DIGITAL DATA

The output of the icing occurrence and reoccurrence overlay model for the Landsat time series (1984 – 2014) of images positioned at WRS-2 Path 49, Row 16, located within the Lac la Martre area, NWT, is presented in this Open File as georeferenced ArcGIS™ Geodatabase format and Shapefile format files. FGDC compliant metadata, included as an XML file, are annotated in Appendix 1.

6 ACKNOWLEDGEMENTS

This work was conducted under the PHASAR (Permafrost and Hydrology in Arctic and Sub Arctic Regions) activity of the Geological Survey of Canada (GSC) at Natural Resources Canada (NRCan), and was developed during Colleen Fish's term as a (RAP) summer student with the GSC.

7 REFERENCES

Carey KL. 1973. *Icings Developed from Surface Water and Ground Water, Cold Regions Science and Engineering Monograph 111-D3*. U.S. Army Cold Regions Research and Engineering Laboratory: Hanover, New Hampshire. 66 p.

Chander G, Markham B, Helder D. 2009. Summary of current radiometric calibration coefficients for Landsat MSS, TM, ETM+, and EO-1 ALI sensors. *Remote Sensing of the Environment*, **113**: 893-903. DOI: 10.1016/j.rse.2009.01.007.

Choi H, Bindschadler R. 2004. Cloud detection in Landsat imagery of ice sheets using shadow matching technique and automated normalized difference show index threshold value decision. *Remote sensing of Environment*, **91**: 237-242. DOI: 10.1016/j.rse.2004.03.007.

Colby DJ. 1991. A review of assessing the accuracy of classifications of remotely sensed data. *Remote Sensing of Environment*, **37**: 35-46. DOI: 10.1016/0034-4257(91)90048-B.

Dean KG. 1984. *Stream-icing zones in Alaska, Alaska Division of Geological & Geophysical Surveys Report of Investigation 84-16*. Alaska Division of Geological & Geophysical Surveys, Fairbanks, Alaska. 20 p., 102 sheets, scale 1:250,000. DOI:10.14509/2375.

Ecosystem Classification Group. 2007. *Ecological Regions for the Northwest Territories – Taiga Plains*. Department of Environment and Natural Resources, Government of the Northwest Territories: Yellowknife, Canada; 173 p.

Ecosystem Classification Group. 2008. *Ecological Regions for the Northwest Territories – Taiga Shield*. Department of Environment and Natural Resources, Government of the Northwest Territories: Yellowknife, Canada; 149 p.

Environment Canada, 2016 *Canadian Climate Normals 1981-2010 Station Data-Yellowknife A*. Temperature and Precipitation. Northwest Territories. http://climate.weather.gc.ca/climate_normals/results_1981_2010_e.html?searchType=stnProv&lstProvince=NT&txtCentralLatMin=0&txtCentralLatSec=0&txtCentralLongMin=0&txtCentralLongSec=0&stnID=1706&dispBack=0

Hall DK, Roswell C. 1981. The origin of water feeding icings on the eastern North Slope of Alaska. *Polar Record*, **20**: 433-438. DOI: http://dx.doi.org/10.1017/S0032247400003648.

Hall DK, Riggs GA, Salomonson VV. 1995. Development of methods for mapping global snow cover using Moderate Resolution Imaging Spectroradiometer (MODIS) data. *Remote Sensing of environment*, **54**: 127-140. DOI: 10.1016/0034-4257(95)00137-P.

Harden D, Barnes P, Reimnitz. 1977. Distribution and character of naleds in northeastern Alaska. *Arctic*, **30**: 28-40.

Heginbottom JA, Dubreuil MA, Harker PA. 1995. Canada-Permafrost. In *National Atlas of Canada*, 5th edition. National Atlas Information Service: Natural Resources Canada, Ottawa, ON; Plate 2.1. MCR 4177.

Jeffries MO, Morris K, Kozlenko N. 2005. Ice characteristics and process, and remote sensing of frozen rivers and Lakes. In *Remote Sensing in Northern Hydrology: Measuring Environmental Change, Geographical Monograph Series 163*, CR Duguay, A Pietroniro (eds.). American Geophysical Union, Washington, DC; 63-90.

Kane DL, 1981. Physical mechanics of aufeis growth. *Canadian Journal of Civil Engineering*, **8**: 186-195. DOI: 10.1139/l81-026.

Kane DL, Slaughter CW. 1973. Seasonal regime and hydrological significance of stream icings in central Alaska. In *Role of Snow and Ice in Hydrology: Proceedings of Symposia held at Banff,*

September 1972, Publication 107, Volume 1. International Association of Hydrological Science, Gentbrugge, Belgium; 528-540.
Kane DL, Yoshikawa K, McNamara JP. 2013. Regional groundwater flow in an area mapped as continuous permafrost, NE Alaska (USA). *Hydrogeological Journal*, **21**: 41-52. DOI: 10.1007/s10040-012-0937-0.
Kerr DE, Wilson P. 2000. *Preliminary surficial geology studies and mineral exploration considerations in the Yellowknife area, Northwest Territories*. Natural Resources Canada, Geological survey of Canada, Current Research 2000-C3 (online: http://nrcan.gc.ca/gsc/bookstore).
Li S, Benson C, Shapiro L, Dean K. 1997. Aufeis in the Ivishak River, Alaska, mapped from satellite radar interferometry. *Remote Sensing of Environment*, **60**: 131-139. DOI: 10.1016/S0034-4257(96)00167-8.
McFeeters SK. 1996. The use of the Normalized Difference Water Index (NDWI) in the delineation of open water features. *International Journal of Remote Sensing* **17**: 1425-1432. DOI: 10.1080/01431169608948714.
Morse, P.D. and Wolfe, S.A., 2014. Icings in the Great Slave Region (1985—2014), Northwest Territories, Mapped from Landsat Imagery; Geological Survey of Canada, Open File 7720, 1 .zip file. doi:10.4095/295540
Morse, P.D., and S.A. Wolfe (2015), Geological and meteorological controls on icing (aufeis) dynamics (1985 to 2014) in subarctic Canada, *J. Geophys. Res. Earth Surf., 120,* doi:10.1002/2015JF003534
Prowse, TD. 1995. River ice processes. In *River Ice Jams*, S Beltaos (ed.). Water Resources Publications, LLC: Highlands Ranch, Colorado; 29-70.
Reedyk S, Woo M-K, Prowse TD. 1995. Contribution of icings ablation to streamflow in a discontinuous permafrost area. *Canadian Journal of Earth Sciences* **32**: 13-20. DOI: 10.1139/e95-002.
Romanovskii NN, Gravis GF, Melnikov ES, Leibman MO. 1996. Periglacial processes as geoindicators in the cryolithozone. In *Geoindicators: Assessing Rapid Environmental Changes in Earth Systems*, AR Berger, WJ Iams (eds.). A.A. Balkema: Rotterdam, Netherlands; 47-67.
Veillette JJ, Thomas RD. 1979. Icings and seepage in frozen glaciofluvial deposits, District of Keewatin, N.W.T. *Canadian Geotechnical Journal*, **16**: 789-798. DOI: 10.1139/t79-084.
Water Survey of Canada, 2016. *Historical Hydrometric Data.* Daily Discharge and Water Level Data Availability for La Martre River Below Outlet of Lac la Martre. http://wateroffice.ec.gc.ca/report/data_availability_e.html?type=h2oArc&station=07TA001&dataType=FlowandLevel
Yoshikawa K, Hinzman LD, Kane DL. 2007. Spring and aufeis (icing) hydrology in Brooks Range, Alaska. *Journal of Geophysical Research* **112**: G04S43. DOI: 10.1029/2006JG000294.
Zhu X, Desheng L, Chen J. 2013. A new geostatistical approach for filling gaps in Landsat ETM+ SLC-off images. *Remote Sensing of Environment*, **124**: 49-60. DOI: 10.1016/j.rse.2012.04.019.
Zhu Z, Woodcock CE. 2012. Object-based cloud and cloud shadow detection in Landsat imagery. *Remote Sensing of Environment*, **118**: 83-94. DOI: 10.1016/j.rse.2011.10.028.

APPENDIX 1

- <metadata>
- <idinfo>
- <citation>
- <citeinfo>
<title>**Icings in the Lac La Martre area (1984-2015), Northwest Territories, Mapped from Landsat Imagery**</title>
<geoform>**vector digital data**</geoform>
</citeinfo>
</citation>
- <descript>
<abstract>**Icing occurrence and reoccurence maps provide important geoscience information required for development and transportation infrastructure planning. This shapefile presents an icing occurence and reoccurence dataset for the time series of Landsat images (1984-2015) positioned at WRS-2 Path 49/Row 16, located within the Lac la Martre area. These data, generated using a maximum difference band ratio approach, provide the first assessment of icing distribution in this area. This preliminary information is required to assess terrain risks to northern transportation infrastructure, and may guide route selection for future transportation corridors within the Bear and Interior Platform Geolocial Provinces.</**abstract>
<purpose>**This dataset presents icing occurence and reoccurence data for the time series of Landsat images (1984-2015) positioned at WRS-2 Path 49/Row 16, located within the Lac la Martre area**</purpose>
</descript>
<bounding>
<westbc>-**120.389348**</westbc>
<eastbc>**-115.842478**</eastbc>
<northbc>**63.831294**</northbc>
<southbc>**61.900617**</southbc>
</bounding>
</spdom>
<keywords>
<theme>
<themekt>**None**</themekt>
<themekey>**Icings**</themekey>
<themekey>**Landsat**</themekey>
<themekey>**Lac la Martre**</themekey>
<themekey>**Whati**</themekey>
<themekey>**Northwest Territories**</themekey>
</theme>
</keywords>
<accconst>**None**</accconst>
<useconst>**Her Majesty the Queen in right of Canada, as represented by the Minister of Natural Resources ("Canada"), does not warrant or guarantee the accuracy or completeness of the information ("Data") and does not assume any responsibility or liability with respect to any damage or loss arising from the use or interpretation of the Data. The Data are intended to convey regional trends and should be used as a guide only. The Data should not be used for design or construction at any specific location, nor are the Data to be used as a replacement for the types of site-specific geotechnical investigations**.</useconst>
<datacred>**Fish, C.S., Morse, P.D., and Wolfe, S.A. 2016. Icings in the Lac la Martre area (1984–2015), Northwest Territories, mapped from Landsat imagery; Geological Survey of Canada, Open File 8124, 1 .zip file. doi:10.4095/299737**</datacred>

<native>**Microsoft Windows 7 Version 6.1 (Build 7601) Service Pack 1; Esri ArcGIS 10.1.1.3143**</native>
</idinfo>
<spdoinfo>
<direct>**Vector**</direct>
<ptvctinf>
<sdtsterm>
<sdtstype>**GT-polygon composed of chains**</sdtstype>
<ptvctcnt>**1131**</ptvctcnt>
</sdtsterm>
</ptvctinf>
</spdoinfo>
<spref>
<horizsys>
<planar>
<mapproj>
<mapprojn>**WGS 1984 UTM Zone 11N**</mapprojn>
<transmer>
<sfctrmer>**0.9996**</sfctrmer>
<longcm>-**117.0**</longcm>
<latprjo>**0.0**</latprjo>
<feast>**500000.0**</feast>
<fnorth>**0.0**</fnorth>
</transmer>
</mapproj>
<planci>
<plance>**coordinate pair**</plance>
<coordrep>
<absres>**0.00000000222002416450095 6**</absres>
<ordres>**0.00000000222002416450095 6**</ordres>
</coordrep>
<plandu>**meter**</plandu>
</planci>
</planar>
<geodetic>
<horizdn>**D WGS 1984**</horizdn>
<ellips>**WGS 1984**</ellips>
<semiaxis>**6378137.0**</semiaxis>
<denflat>**298.257223563**</denflat>
</geodetic>
</horizsys>
</spref>
<eainfo>
<detailed>
<enttyp>
<enttypl>**LLMA_Icings_1984to2015_OF_xxxx**</enttypl>
</enttyp>
<attr>
<attrlabl>**FID**</attrlabl>
<attrdef>**Internal feature number**.</attrdef>
<attrdefs>**Esri**</attrdefs>
<attrdomv>
<udom>**Sequential unique whole numbers that are automatically generated**.</udom>
</attrdomv>
</attr>
<attr>

<attrlabl>**Shape**</attrlabl>
<attrdef>**Feature geometry.**</attrdef>
<attrdefs>**Esri**</attrdefs>
<attrdomv>
<udom>**Coordinates defining the features**.</udom>
</attrdomv>
</attr>
<attr>
<attrlabl>**Frequency**</attrlabl> [Number: Icing return frequency at that polygon]
</attr>
<attr>
<attrlabl>**Aggregator**</attrlabl>[Number: Icing aggregation ID, indicates unique icing, may be composed of polygons]
</attr>
<attr>
<attrlabl>**Area_km_**</attrlabl> [Number: Area of polygon in km]
</attr>
<attr>
<attrlabl>**ECO4_NAME**</attrlabl>[Text indicating one of ten possible attributes: Lac Grandin Upland Low Subarctic; Lac Grandin Plain Low Subarctic; Bulmer Plain Low Subarctic; Great Slave Lowland High Boreal; Great Slave Upland High Boreal; Great Slacve Plain High Boreal; Horn Slopes Low Subarctic; Horn Plateau Low Subarctic; Horn Slopes Mid Boreal; and Great Slave Lowland Mid Boreal]
</attr>
<attr>
<attrlabl>**1984**</attrlabl>[Binary value : 1 indicates icing present, 0 indicates no icing present]
</attr>
<attr>
<attrlabl>**1991**</attrlabl>[Binary value : 1 indicates icing present, 0 indicate no icing present]
</attr>
<attr>
<attrlabl>**1985**</attrlabl>[Binary value : 1 indicates icing present, 0 indicate no icing present]
</attr>
<attr>
<attrlabl>**1992**</attrlabl>[Binary value : 1 indicates icing present, 0 indicate no icing present]
</attr>
<attr>
<attrlabl>**1993**</attrlabl>[Binary value : 1 indicates icing present, 0 indicate no icing present]
</attr>
<attr>
<attrlabl>**1994**</attrlabl>[Binary value : 1 indicates icing present, 0 indicate no icing present]
</attr>
<attr>
<attrlabl>**1996**</attrlabl>[Binary value : 1 indicates icing present, 0 indicate no icing present]
</attr>
<attr>
<attrlabl>**1998**</attrlabl>[Binary value : 1 indicates icing present, 0 indicate no icing present]
</attr>
<attr>
<attrlabl>**1999**</attrlabl>[Binary value : 1 indicates icing present, 0 indicate no icing present]
</attr>
<attr>
<attrlabl>**2000**</attrlabl>[Binary value : 1 indicates icing present, 0 indicate no icing present]
</attr>
<attr>
<attrlabl>**2001**</attrlabl>[Binary value : 1 indicates icing present, 0 indicate no icing present]

</attr>
<attr>
<attrlabl>**2002**</attrlabl>[Binary value : 1 indicates icing present, 0 indicate no icing present]
</attr>
<attr>
<attrlabl>**2004**</attrlabl>[Binary value : 1 indicates icing present, 0 indicate no icing present]
</attr>
<attr>
<attrlabl>**2005**</attrlabl>[Binary value : 1 indicates icing present, 0 indicate no icing present]
</attr>
<attr>
<attrlabl>**2006**</attrlabl>[Binary value : 1 indicates icing present, 0 indicate no icing present]
</attr>
<attr>
<attrlabl>**2008**</attrlabl>[Binary value : 1 indicates icing present, 0 indicate no icing present]
</attr>
<attr>
<attrlabl>**2009**</attrlabl>[Binary value : 1 indicates icing present, 0 indicate no icing present]
</attr>
<attr>
<attrlabl>**2010**</attrlabl>[Binary value : 1 indicates icing present, 0 indicate no icing present]
</attr>
<attr>
<attrlabl>**2011**</attrlabl>[Binary value : 1 indicates icing present, 0 indicate no icing present]
</attr>
<attr>
<attrlabl>**2013**</attrlabl>[Binary value : 1 indicates icing present, 0 indicate no icing present]
</attr>
<attr>
<attrlabl>**2014**</attrlabl>[Binary value : 1 indicates icing present, 0 indicate no icing present]
</attr>
<attr>
<attrlabl>**2015**</attrlabl>[Binary value : 1 indicates icing present, 0 indicate no icing present]
</attr>
</detailed>
</eainfo>
<metainfo>
<metd>**20160822**</metd>
<metstdn>**FGDC Content Standard for Digital Geospatial Metadata**</metstdn>
<metstdv>**FGDC-STD-001-1998**</metstdv>
<mettc>**local time**</mettc>
</metainfo>
</metadata>